S & M 4244

# Sensor-assisted Vibratory Stress Relief Using Resonant Excitation and X-ray Diffraction Monitoring for Sustainable Manufacturing

Shih-Chuan Cheng\* and Rong-Shean Lee

Department of Mechanical Engineering, National Cheng Kung University, No. 1, University Road, East District, Tainan City 701, Taiwan (R.O.C.)

(Received July 1, 2025; accepted November 6, 2025)

*Keywords:* sensor-assisted stress monitoring, vibratory stress relief, X-ray diffraction stress measurement, sustainable manufacturing

In this study, we present a sustainable, sensor-assisted method for relieving residual stress in interference-fitted metal components, integrating press-fitting and vibratory stress relief at the component's natural frequency. The process is structured into four stages: (1) initial residual stress and geometric alignment assessment via X-ray diffraction (XRD) and alignment sensors, (2) the identification of the workpiece's resonant frequency using a vibration analyzer, (3) the application of controlled resonant excitation to induce stress relaxation, and (4) the re-evaluation of residual stress and perpendicularity after treatment. Experimental results demonstrated effective stress redistribution, resulting in a significant reduction in residual stress and improved dimensional stability, particularly at higher interference strains. The integrated use of vibration sensing and XRD confirmed microstructural recovery through reduced full width at half maximum values of diffraction peaks, which means the reduction in dislocation density. This nondestructive, energy-efficient approach supports sustainable manufacturing by enhancing product reliability without material removal.

### 1. Introduction

A disk-pin-assembled turning workpiece was observed to exhibit increasing vibration intensity during operation, raising concerns about product vibration and service life. The abnormal vibration behavior was suspected to result from residual stress relief occurring during operation, which may have altered the perpendicularity of the disk-pin and contributed to progressive dynamic unbalance distortion. These observations underscore the necessity for a reliable and nondestructive stress relief method that can preserve both mechanical integrity and dimensional accuracy in interference-fitted assemblies.

Residual stress commonly arises from manufacturing processes such as machining, welding, and mechanical joining. (1) Dislocations are linear defects that form when a material undergoes plastic deformation beyond its yield strength. These defects enable atoms to slip along specific

\*Corresponding author: e-mail: <u>n18061054@gs.ncku.edu.tw</u> <u>https://doi.org/10.18494/SAM5836</u>

planes, allowing a permanent change in shape with less energy. As deformation continues, dislocations multiply and interact, generating complex internal stress fields. When deformation is uneven across the material, these internal strains do not fully relax, resulting in residual stress that remains even after the external load is removed. (2-4) In our case, the disk component was fabricated by a deep-drawn process, which introduces substantial residual stress due to the buildup of dislocations in a chain of plastic deformation. If left unrelieved, these internal stresses can lead to geometric distortion, premature fatigue failure, and reduced service life, (5-7) particularly in thin-walled or assembled components. Conventional stress relief techniques—such as thermal annealing and mechanical shot peening (8)—are often energy-intensive, time-consuming, and inapplicable to fully assembled structures, where maintaining precise tolerances is crucial. In contrast, press-fitting has been shown to partially relieve residual stress through controlled plastic deformation at the interference interface, offering a practical, assembly-compatible alternative for stress management. (9)

Vibratory stress relief (VSR) provides a nondestructive and energy-efficient alternative to conventional thermal methods by applying controlled mechanical excitation. This excitation promotes internal stress redistribution through localized plastic deformation and dislocation movement, allowing residual stress to relax without altering the material's geometry or mechanical properties. (10,11) Although press-fitting can induce plastic deformation that contributes to partial residual stress relief, it may not always reduce the stress to a sufficient level, particularly in areas of high constraint or stress concentration. (9,12) To overcome this limitation, in this study, we employ VSR following press-fitting to assess its potential for improving stress relief. While VSR has been effectively applied in welded and cast components, (13) its use in press-fit assemblies and precision-fitted parts remains limited, presenting a valuable opportunity for research and industrial applications.

X-ray diffraction (XRD) is a reliable technique for assessing the effectiveness of VSR by analyzing residual stress and microstructural changes. After VSR treatment, XRD measurements typically show a reduction in residual stress level, confirming successful stress relaxation. Additionally, a decrease in the full width at half maximum (*FWHM*) of diffraction peaks indicates reductions in micro-strain and dislocation density. This decrease reflects the dislocation rearrangement and partial recovery of the crystal structure. Together, the reductions in residual stress and *FWHM* measured by XRD provide clear, nondestructive evidence of the stress-relieving effects of VSR. (14,15) VSR has been shown to reduce *FWHM* by approximately 10–14%, indicating decreased nonuniform strain and residual stress in rolled alloys. Peak intensity and width change significantly after vibration, suggesting improved strain uniformity. These results demonstrate that VSR promotes internal stress relaxation and dislocation rearrangement, leading to narrower diffraction peaks in XRD analysis and improved microstructural stability. (16)

In this study, we investigated the residual stress relief behavior of press-fitted steel components subjected to various interference strain levels, followed by the application of VSR. A sensor-assisted approach is employed to monitor changes in residual stress and perpendicularity deviation, allowing for the evaluation of both internal stress redistribution and geometric stability. Both press-fitting and VSR are inherently sustainable processes, as they

involve no material removal, generate no waste, and consume significantly low energy compared with conventional thermal or machining-based stress relief methods.<sup>(2)</sup> The objective of this study is to assess the combined effectiveness of these two methods in reducing residual stress to a sufficient level while maintaining dimensional accuracy. The findings aim to validate a practical, low-impact VSR technique suitable for precision-fitted assemblies, supporting cleaner manufacturing practices and improved product reliability.

# 2. Materials and Experimental Methods

In this section, we outline the materials used, press-fit configurations, and experimental procedures for evaluating residual stress and perpendicularity. We describe in detail the natural frequency identification, the VSR process, and the measurement techniques employed to assess the effectiveness of stress reduction and geometric stability.

## 2.1 Materials and setup of the press-fitted workpiece

Figure 1 shows the press-fitting assembly consisting of a shaft and a plate with a matching hole, designed to investigate the effects of varying interference fits on residual stress and structural deformation. The shaft, fabricated from SUJ2 alloy steel, had a diameter of 2.99 mm, whereas the plate, made of C1002 low-carbon steel, featured hole diameters of 2.96, 2.95, and 2.93 mm. The outer diameter of the plate was 20 mm. These hole sizes corresponded to radial strain ( $\mathcal{E}r$ ) values of 1.00, 1.30, and 2.01%, respectively.<sup>(9)</sup>

#### 2.2 Experimental methods

Figure 2 shows the experimental procedure, which involves four main steps. First, the initial residual stress and perpendicularity of the workpiece were measured. Next, the natural frequency

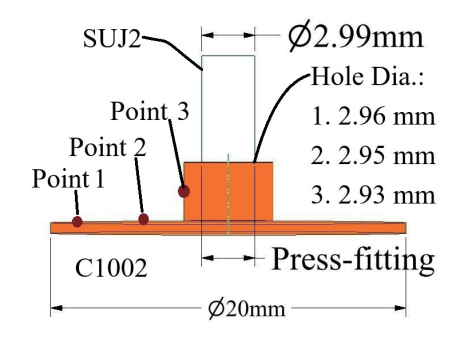


Fig. 1. (Color online) Materials and dimensions of the workpiece.

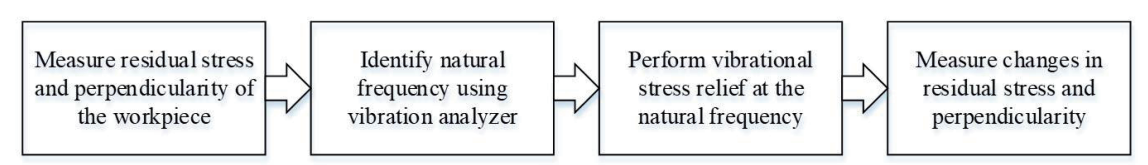


Fig. 2. Experimental methods.

of the workpiece was identified using a vibration analyzer. Vibrotary stress relief was then applied by exciting the workpiece at its natural frequency. Finally, the residual stress and perpendicularity were measured again to assess the effectiveness of the stress relief process.

#### 2.2.1 Residual stress measurement before VSR

Residual stresses were measured using a Proto iXRD® portable X-ray diffraction system equipped with a Cr-K $\alpha$  radiation source ( $\lambda$  = 2.2897 Å) and a vanadium K- $\beta$  filter. The measurements followed the  $\sin^2 \psi$  method in accordance with ASTM E915-21. A one-dimensional position-sensitive scintillation detector and a goniometer with a  $\psi$ -tilt stage were used to record diffraction data over multiple  $\psi$  orientations ranging from –45 to +45°. The X-ray tube operated at 25 kV and 5 mA. A 1 mm collimator was selected to achieve high spatial resolution. The ferrite {211} plane of the body-centered cubic (BCC) structure was analyzed at an approximate 20 angle of 156.1°. Each measurement point was irradiated for 5 s per  $\psi$ -step, and the resulting diffraction peaks were fitted with a pseudo-Voigt function to determine the precise 20 position and WHM after correcting for instrumental broadening. The X-ray elastic constant was taken as 175 GPa, and stresses were calculated from the linear relationship between lattice strain and  $\sin^2 \psi$ . (9)

In the Proto iXRD residual stress analyzer, FWHM is determined directly from the diffraction peak obtained during the X-ray scan for each  $\psi$  tilt. After background subtraction, the system's analysis software fits the diffraction intensity curve using a pseudo-Voigt function, which combines Gaussian and Lorentzian components to represent both instrumental and microstructural broadening processes. From this fitted peak, the maximum intensity  $I_{max}$  is identified, and the software calculates the angular positions  $\theta_1$  and  $\theta_2$  at which the intensity equals half of the peak maximum  $(I(\theta) = I_{max} / 2)$ . FWHM is then computed as the difference between these two positions, expressed mathematically as  $FWHM = 2(\theta_2 - \theta_1)$ . (17,18)

This configuration allowed the accurate evaluation of residual stresses before and after VSR, providing reliable insight into stress redistribution and microstructural relaxation in ferritic steel components.

## 2.2.2 Perpendicularity measurement before VSR

Before applying VSR, the initial perpendicularity of the workpiece was measured to establish a baseline for evaluating geometric changes. This measurement was conducted using a high-precision alignment instrument capable of detecting slight deviations in angularity between the workpiece surfaces. Ensuring accurate initial perpendicularity data was essential for assessing the potential impact of the VSR process on the dimensional stability of the component.

After the VSR treatment, perpendicularity was measured again under identical conditions, and the deviation rate of perpendicularity was calculated to quantify the extent of geometric change. The deviation rate was defined as the ratio of the post-VSR perpendicular deviation (Post-VSR perp. dev.) to the pre-VSR perpendicular deviation (Pre-VSR perp. dev.), expressed as

$$Deviation \ rate (\%) = \frac{(Post - VSR \ perp. dev.) - (Pre - VSR \ perp. dev.)}{Pre - VSR \ prep. dev.} \times 100\%. \tag{1}$$

A lower deviation rate indicates that the perpendicularity remained closer to its original state, meaning that the geometry changed less after VSR and thus exhibited higher dimensional stability. This parameter is plotted in Fig. 11 to compare the geometric stabilities of workpieces under different interference strain conditions.

## 2.2.3 Natural frequency identification

To determine the natural frequency of the workpiece, an impact test was conducted using a metal exciter, which delivered a sharp tap to the component's surface. The resulting vibrational response was captured by an accelerometer connected to a vibration analyzer (e.g., the Novian system), which recorded the time-domain signal and converted it into a frequency spectrum using the fast Fourier transform (FFT). The peak in the frequency spectrum corresponding to the dominant response was identified as the natural frequency of the workpiece. This frequency was then used as the excitation input for the subsequent VSR process.

# 2.2.4 VSR at natural frequency

VSR was performed by exciting workpieces at their previously identified natural frequencies using an external vibration generator. The excitation was applied for a controlled duration, ensuring that the vibration amplitude remained within a safe range to avoid any structural damage. The setup was designed to maintain stable contact and consistent excitation, allowing the internal stresses within the material to redistribute gradually over time.

During VSR, the vibration amplitude was quantitatively controlled and monitored using a triaxial accelerometer mounted on the plate surface. The amplitude was maintained at approximately 680 mg<sub>(rms)</sub> at 24 Hz, which provided sufficient excitation energy for stress redistribution while preventing excessive dynamic loading. The amplitude was adjusted by varying the excitation voltage of the vibration generator until the target range was reached and kept constant throughout the 30 min VSR process.

# 2.2.5 Final residual stress and perpendicularity measurement after VSR

After the VSR process, both the residual stress and perpendicularity of the workpiece were remeasured to evaluate the effectiveness of the treatment. The residual stress was assessed using the same method and equipment as in the initial measurement to ensure consistency and comparability. Perpendicularity was measured using a precision alignment tool to detect any geometric changes that may have occurred during the process. These post-treatment measurements provided critical data for determining the extent of stress reduction and any improvements or distortions in the workpiece geometry resulting from the VSR process.

## 3. Results and Discussion

In this section, we present the experimental findings on the behavior of residual stress and dimensional stability before and after VSR. We analyze the effects of interference strain, stress redistribution, and microstructural changes, supported by X-ray diffraction and geometric measurements across multiple locations on the workpiece.

# 3.1 Natural frequency measurement and performing VSR at 2X frequency

Figure 3 presents the natural frequency detection results for workpieces subjected to three different radial strain levels:  $\mathcal{E}r=1.00,\ 1.30,\$ and 2.01%. Despite the varying degrees of interference fit, all specimens exhibited a consistent peak response at approximately 12 Hz, indicating that the induced strain had minimal effects on the workpiece's dynamic characteristics. The uniformity of the frequency response curves across all three conditions suggests that the structural stiffness and mass distribution of the system remained essentially unchanged. This stability in natural frequency is crucial for the VSR process, as it confirms that a single resonant excitation frequency of 12 Hz can be effectively applied to all specimens, ensuring consistent and reliable stress relief performance regardless of the interference level.

The VSR process was conducted at approximately twice the natural frequency of the workpiece at around 24 Hz, based on the 12 Hz natural frequency identified and maintained for 30 min. Figure 4 illustrates the VSR excitation condition applied during the experiment.

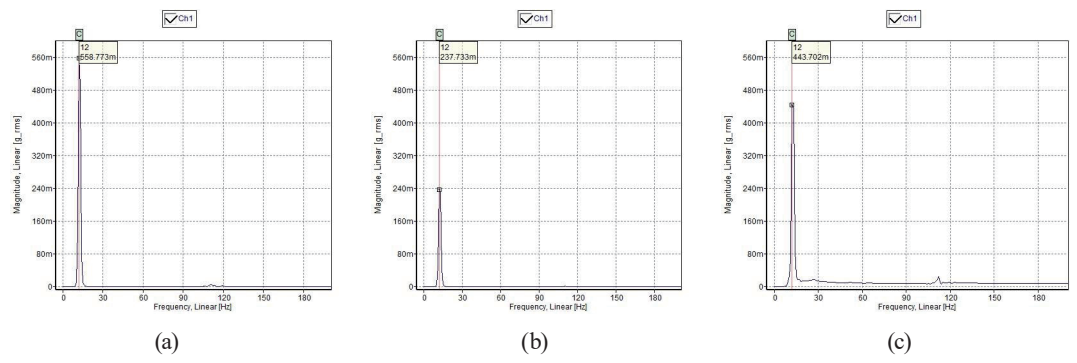


Fig. 3. (Color online) Natural frequency detection using vibration sensor of  $\mathcal{E}_r = (a) 1.00$ , (b) 1.30, and (c) 2.01%.

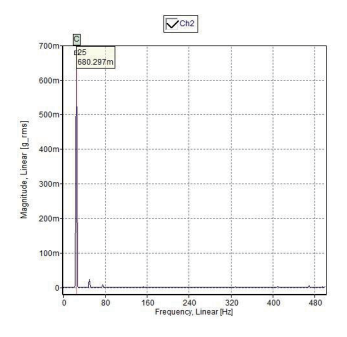


Fig. 4. VSR performed at roughly 2× frequency.

Operating at the second harmonic allowed for enhanced energy input and a more effective excitation of the structure while keeping the vibration amplitude within a safe range. This approach ensured broader modal activation and more uniform internal stress redistribution. The 30 min treatment period provided sufficient time for stress relaxation without causing structural damage or overheating. The results confirm that the VSR excitation was carefully controlled in both frequency and duration, enabling reliable and consistent residual stress relief across all interference strain conditions.

## 3.2 Changes in residual stress after press-fitting and VSR

At Point 1, the changes in residual stress after VSR demonstrated the method's effectiveness in reducing stress even in regions distant from the press-fit interface. As shown in Fig. 5(a), the residual stress decreased consistently across all strain levels following VSR, indicating that the resonant excitation allowed the internal stress fields to redistribute and partially relax. Although Point 1 was not directly deformed during press-fitting, it experienced stress accumulation due to mechanical constraint and structural continuity. The reduction in residual stress suggested that the vibrational energy propagated to this remote region and provided sufficient input to overcome internal resistance, allowing the material to reach a more stable stress state.

Additionally, Fig. 5(b) shows that FWHM also decreased after VSR, indicating microstructural recovery such as reduced lattice distortion and dislocation density. This supported the interpretation that VSR not only relieved macroscopic residual stress but also improved the internal crystal structure. Together, the decreases in both residual stress and FWHM confirmed that VSR effectively alleviated the indirect stress accumulation at Point 1 caused by press-fitting

Figure 6 shows the residual stress and stress relief rate at Point 1 after press-fitting and VSR, respectively. After press-fitting, as shown in Fig. 6(a), the residual stress slightly increased with higher interference strain, and the stress relief rate remained low or even negative, indicating

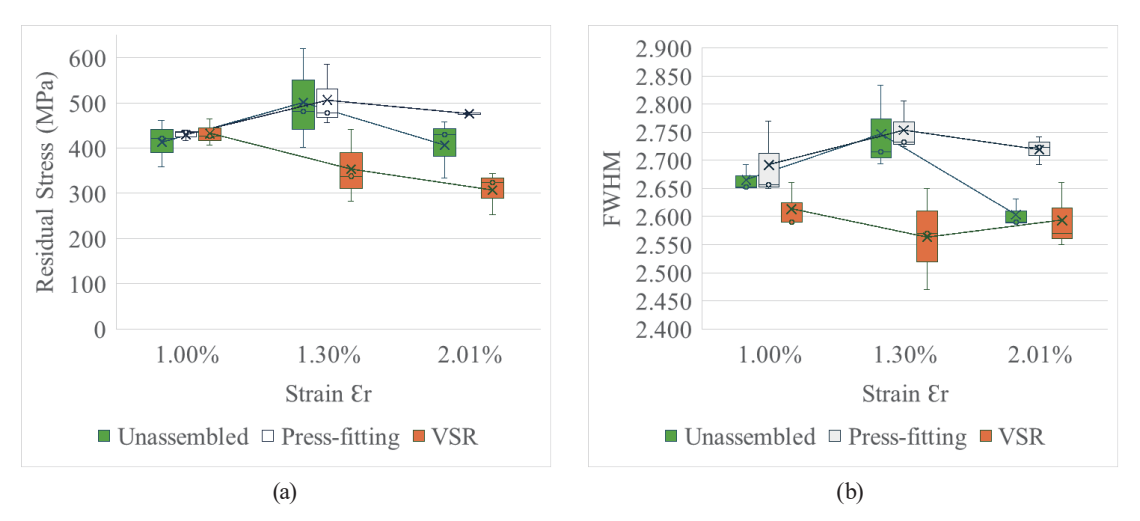


Fig. 5. (Color online) At Point 1, changes in (a) residual stress<sup>(9)</sup> and (b) FWHM vs strain.

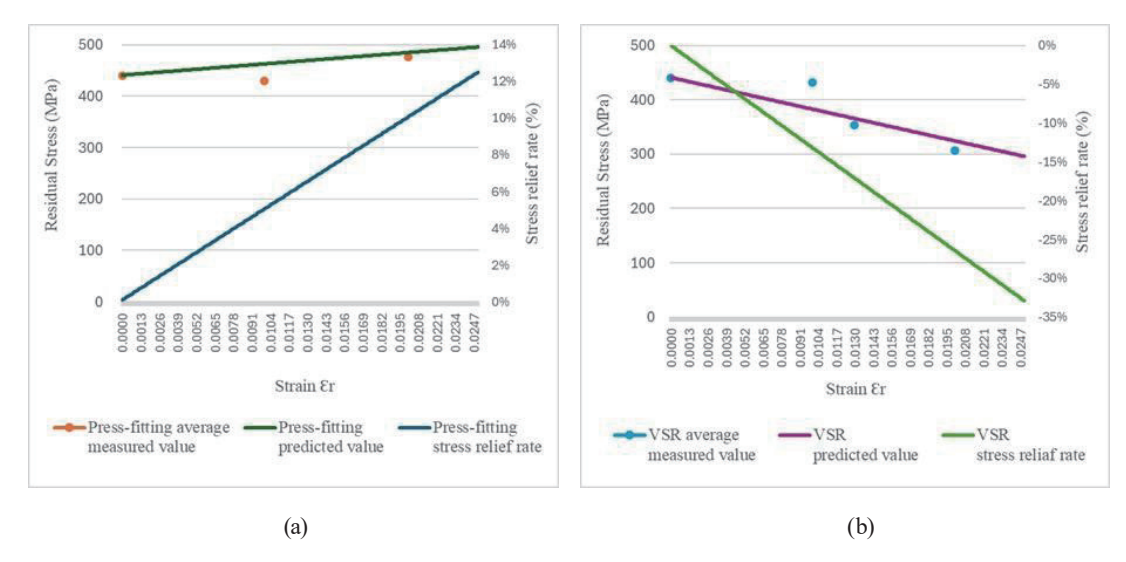


Fig. 6. (Color online) At Point 1, changes in residual stress and stress relief rate after (a) press-fitting<sup>(9)</sup> and (b) press-fitting and VSR.

that press-fitting alone did not relieve stress at this location. In contrast, Fig. 6(b) shows that VSR consistently reduced residual stress across all strain levels, with the stress relief rate becoming positive and increasing with strain. These results demonstrate that while press-fitting caused stress buildup, VSR effectively alleviated residual stress at Point 1 through internal stress redistribution.

In Fig. 7(a), residual stress clearly increased with interference strain after press-fitting, reflecting stress accumulation near the press-fit boundary due to both expansion and constraint effects. After applying VSR, the residual stress showed a slight reduction, but the changes were not significant, indicating that the stress relief at this location was limited. This suggests that Point 2, being in a transitional stress zone, may not fully respond to VSR owing to its mixed stress state and proximity to rigid constraints.

In contrast, Fig. 7(b) shows a more notable trend in the microstructural response. *FWHM* increased after press-fitting, indicating higher dislocation density and lattice distortion. Following VSR, *FWHM* decreased, suggesting partial microstructural recovery despite the modest change in macroscopic stress. These results suggest that while VSR had a limited mechanical stress-relieving effect at Point 2, it still contributed to improving the internal microstructure.

At Point 2, although the macroscopic residual stress reduction after VSR was relatively small, the underlying mechanism can be better understood through microstructural evidence. This transitional region, situated between the highly deformed press-fit interface and the elastic outer zone, experienced competing tensile and compressive components that limited the local mobility of dislocations and constrained lattice relaxation during VSR. As a result, the stress relief was partial rather than complete. Nevertheless, the observed decrease in *FWHM* after VSR indicates that microstructural recovery occurred, involving partial dislocation annihilation and the rearrangement of distorted subgrains. This implies that even in geometrically constrained regions with limited macroscopic stress relaxation, VSR still facilitated localized lattice strain

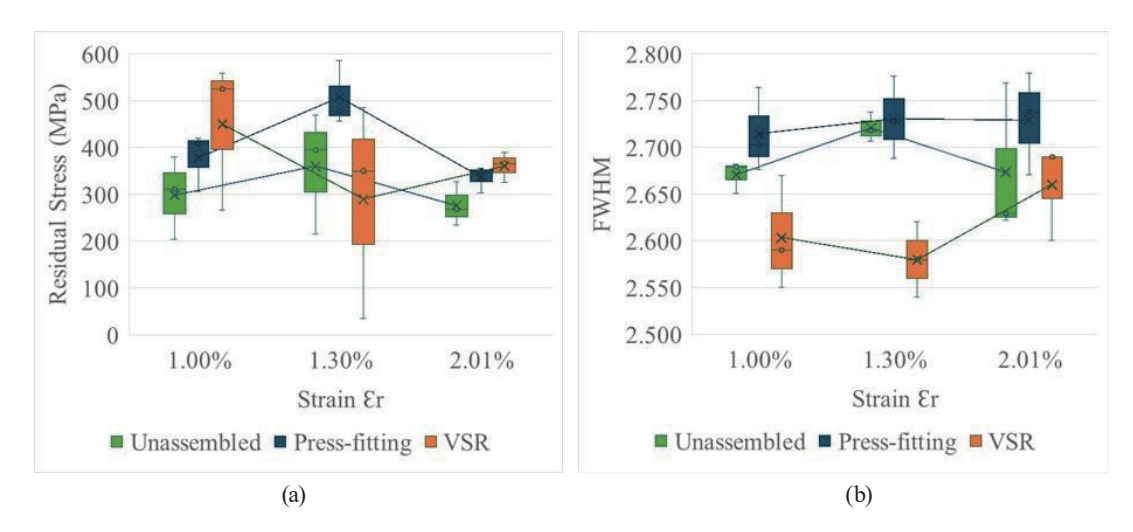


Fig. 7. (Color online) At Point 2, changes in (a) residual stress<sup>(9)</sup> and (b) FWHM vs strain.

recovery and energy redistribution at the microstructural level. Therefore, the combined analysis of residual stress and *FWHM* confirms that transitional regions underwent partial relaxation, governed by a balance between geometric constraint, stress heterogeneity, and the vibrational energy transmitted during resonant excitation.

In Fig. 8(a), the residual stress increased with greater interference strain after press-fitting. This stress buildup is attributed to Point 2's proximity to the press-fit boundary, where the material is subjected to both radial expansion and mechanical constraint. As a result, this region experienced a concentration of tensile stress, and the stress relief rate remained low or even negative, indicating that press-fitting alone was insufficient to mitigate residual stress at this location.

In Fig. 8(b), after VSR, the residual stress showed a slight decrease, but the reduction was not significant. The corresponding stress relief rate remained relatively low, suggesting that VSR had limited effectiveness in alleviating stress at Point 2. This may be due to the complex stress state or insufficient vibrational energy reaching this zone. Overall, while VSR contributed to some improvement, its impact at Point 2 was minimal compared with other areas that were more directly affected by the excitation.

Figure 9(a) shows the changes in residual stress and FWHM at Point 3, located directly at the press-fit interface, concerning increasing strain. After press-fitting, the residual stress had already shown a significant decrease owing to the plastic deformation induced by the tight interference fit, which effectively counteracted the pre-existing tensile stress. However, after applying VSR, the residual stress was further reduced, indicating that VSR provided an additional relaxation effect beyond what was achieved by mechanical fitting alone. The enhanced reduction suggests that while press-fitting introduced beneficial plastic strain, it did not entirely eliminate the internal stress. The resonant excitation from VSR allowed the remaining stress to redistribute and relax more uniformly, further decreasing the residual stress at this critical location.

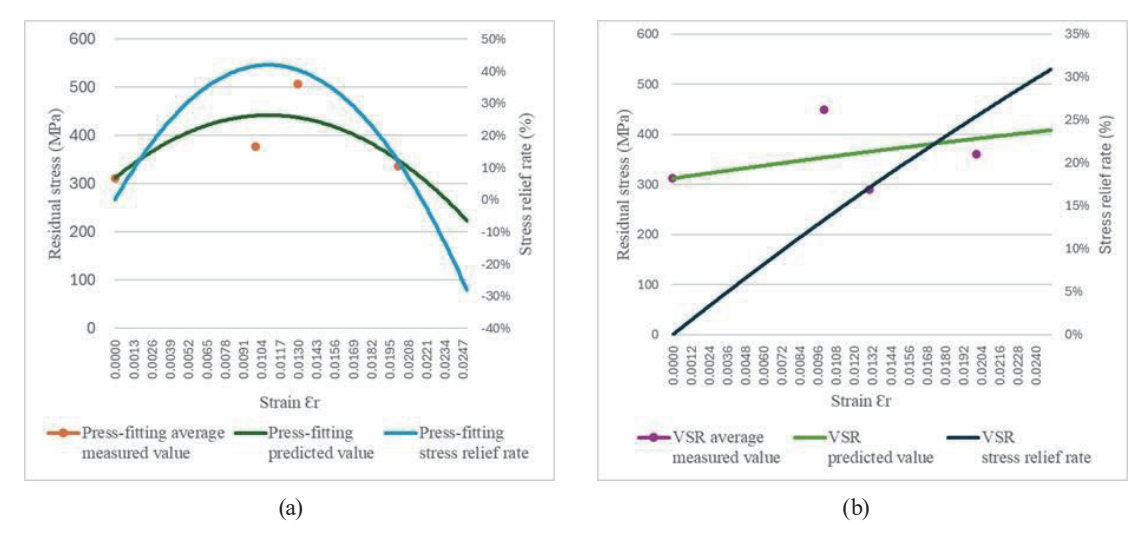


Fig. 8. (Color online) At Point 2, changes in residual stress and stress relief rate after (a) press-fitting(9) and (b) press-fitting & VSR.

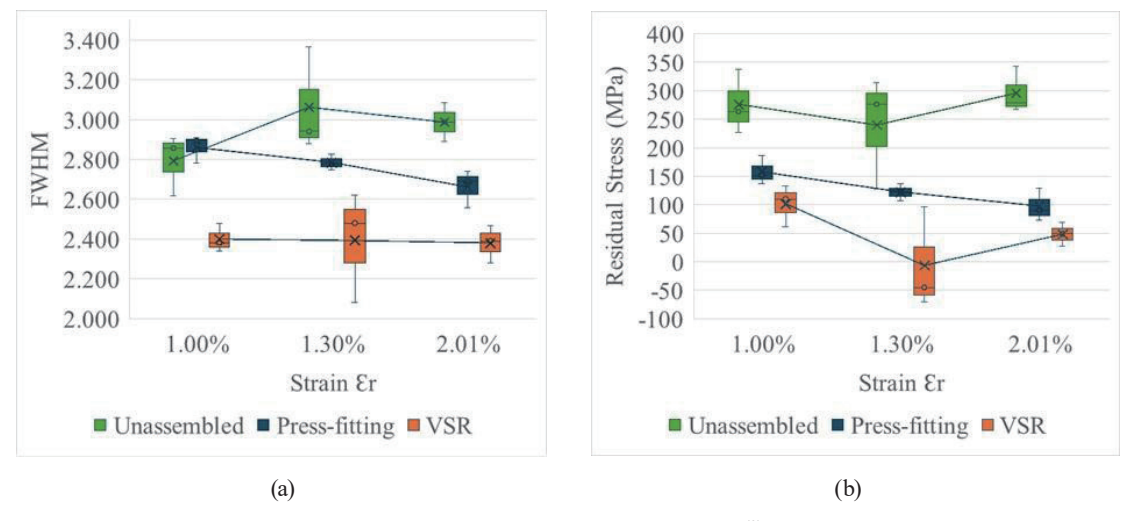


Fig. 9. (Color online) At Point 3, changes in (a) residual stress<sup>(9)</sup> and (b) FWHM vs strain.

Similarly, as shown in Fig. 9(b), FWHM decreased further after VSR, indicating not only mechanical stress relief but also continued microstructural recovery, such as a reduction in dislocation density. This phenomenon, observed in our work with different materials, aligns with previous findings by Wang et al., (16) who demonstrated that VSR reduces FWHM and promotes internal stress relaxation across various alloys. Therefore, at Point 3, where initial stress relief from press-fitting was already substantial, VSR still played a vital role in achieving deeper residual stress and lattice strain reduction.

In Fig. 10(a), after press-fitting, residual stress at Point 3 decreased significantly with increasing interference strain. This substantial stress reduction occurred because Point 3 is located directly at the press-fit interface, where plastic deformation was most intense. The compressive strain introduced by the tight fit effectively neutralized the pre-existing tensile residual stress, making press-fitting highly effective at this location. The stress relief rate was

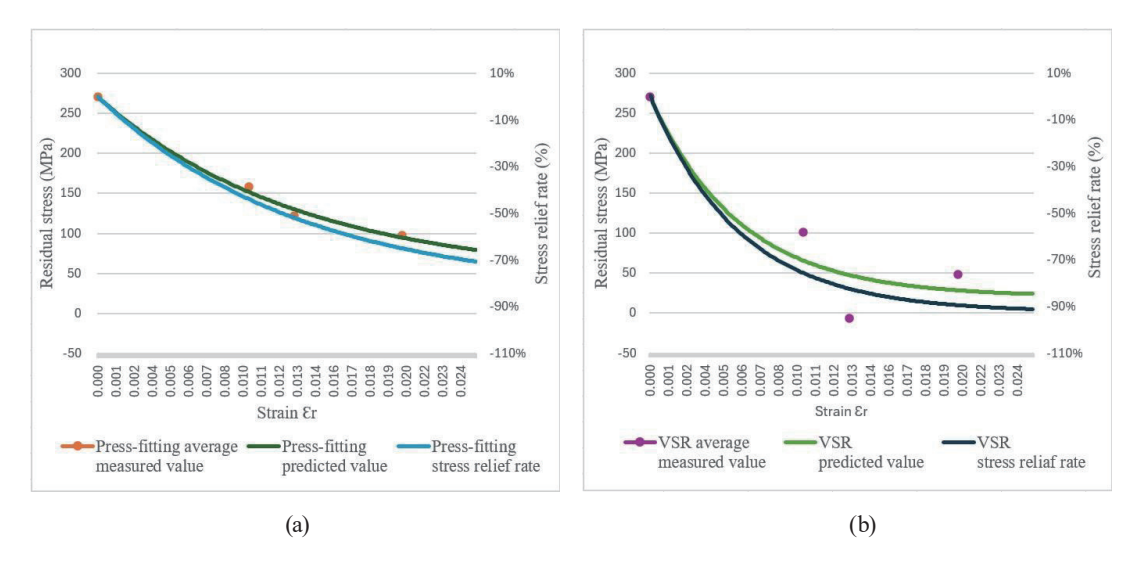


Fig. 10. (Color online) At Point 3, changes in residual stress and stress relief rate after (a) press-fitting<sup>(9)</sup> and (b) press-fitting and VSR.

correspondingly high and increased with strain, reflecting the direct effect of plastic deformation on stress reduction.

In Fig. 10(b), the residual stress reached its lowest value at an interference strain of 1.30%, after which it increased slightly as the interference level continued to rise. This behavior suggests that the reduction in residual stress became saturated near 1.30%, beyond which additional deformation during press-fitting introduced new residual stresses. After applying VSR, the residual stress decreased further, indicating that the vibratory excitation promoted additional relaxation beyond the mechanical effects of press-fitting. This implies that VSR effectively redistributed the remaining internal stresses and refined the stress state introduced by the interference process. Overall, at Point 3, both press-fitting and VSR were effective in achieving stress mitigation, with VSR contributing an additional level of residual stress reduction following the saturation stage.

The relatively large error observed in Fig. 10(b) arises because the residual stresses after VSR were close to zero, producing a flatter  $\sin^2 \psi$  slope and consequently a higher relative uncertainty in the regression analysis. In addition, the high sensitivity of the Proto iXRD system causes larger relative errors when measuring low residual stress values, as even minor variations in diffraction peak position result in amplified stress fluctuations. Furthermore, minor microstructural heterogeneity near the press-fit interface and the propagation of elastic-constant uncertainty contributed to increased data variance. The combined effect of these factors accounts for the larger confidence intervals presented in Fig. 10(b), even though the absolute measurement precision of the Proto iXRD system remained within its specified tolerance. The average residual stress values and their corresponding standard deviations derived from repeated measurements are summarized in Table 1 for reference.

Table 1 Average residual stress and error at point 3 after VSR.

| -                          | _                             |           |
|----------------------------|-------------------------------|-----------|
| Strain $\mathcal{E}_r$ (%) | Average Residual Stress (MPa) | Error (±) |
| 0.00                       | 270                           | 107       |
| 1.00                       | 101                           | 36        |
| 1.30                       | -7                            | 84        |
| 2.01                       | 49                            | 21        |

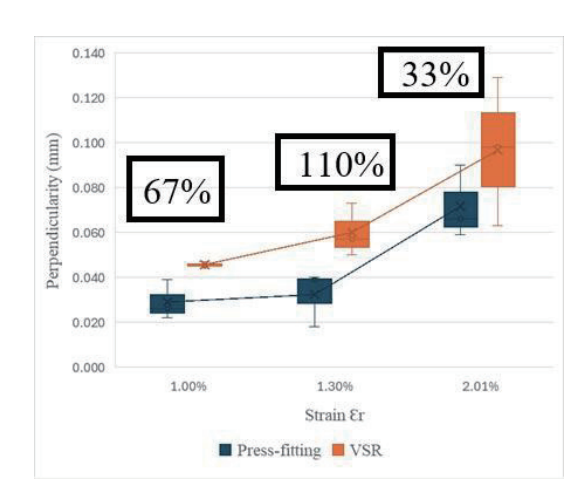


Fig. 11. (Color online) Changes in perpendicularity after press-fitting and VSR.

## 3.3 Changes in perpendicularity after VSR

Figure 11 shows that after VSR, all samples exhibited improved perpendicularity, but the degree of change varied by strain level. At strain values of 1.00 and 1.30%, the deviation decreased notably after VSR, indicating that significant residual stress remained after pressfitting, which, when relieved, caused visible geometric correction. In contrast, at a strain of 2.01%, the perpendicular deviation changed the least after VSR. This is because the residual stress had already been significantly reduced by the press-fitting itself—as shown in earlier figures—particularly at Point 3 where plastic deformation was most effective. As a result, there was less residual stress to release, and therefore less dimensional change during VSR. This minimal deviation implies that the 2.01% strain not only provided better stress relief during press-fitting but also resulted in a more dimensionally stable structure, requiring minimal correction during VSR. Thus, the 2.01% strain yielded the most favorable outcome in terms of both stress relief and geometric stability.

Residual stress and perpendicularity were strongly affected by both interference strain level and measurement location before and after VSR. Among the three measurement points, Point 3, located at the direct press-fitting interface, exhibited the most effective residual stress relief across all strain conditions. This was due to the substantial plastic deformation induced during the interference fit, which significantly reduced internal tensile stress. The effect was further enhanced by VSR, which promoted additional stress redistribution and microstructural recovery. In contrast, Points 1 and 2, located farther from the direct interface, showed less pronounced

stress relief, with some strain-dependent variation. Notably, the 2.01% interference strain condition demonstrated the best overall performance, showing both the lowest residual stress after VSR and the slightest change in perpendicularity, indicating high dimensional stability. These results confirm that both the location of stress and the magnitude of interference strain play critical roles in determining the effectiveness of stress relief.

## 4. Conclusions

In this study, we confirmed that the integration of press-fitting and resonant VSR forms an effective sensor-assisted methodology for sustainable residual stress mitigation in interference-fitted assemblies. The application of VSR at approximately twice the natural frequency resulted in significant stress redistribution and the reduction in dislocation density, as confirmed by both residual stress measurements and the XRD analysis of *FWHM*. By leveraging natural frequency excitation and in situ XRD sensing, the approach enables internal stress redistribution and microstructural recovery without material removal or excessive energy consumption. Among the tested conditions, a 2.01% interference strain achieved the optimal balance between stress relief and dimensional stability. Compared with traditional thermal methods, this combined technique is faster, greener, and compatible with precision assemblies. The findings validate a viable pathway for innovative and sustainable stress management, aligning with ESG principles and offering significant implications for high-precision, eco-efficient manufacturing.

However, certain limitations should be acknowledged. This study was conducted on small-scale components under controlled laboratory conditions, which may not fully represent complex industrial assemblies. Additionally, only one mode of resonant excitation was examined, and the effect of multi-mode or broadband vibration remains to be investigated. Future work will focus on performing accelerated lifetime tests of rotating products treated by the proposed integration of press-fitting and VSR to evaluate long-term durability, fatigue resistance, and dimensional stability under real operational conditions. These investigations will further verify the industrial applicability and robustness of the proposed method.

## Acknowledgments

3D-FLRS International Co., Ltd. supported this work. The authors gratefully acknowledge the company's generous provision of resources, expertise, and technical support, which played a vital role in the successful completion of this project. Their commitment to innovation considerably enriched the quality and scope of the study. The authors also extend their sincere thanks to Professor Jo-Peng Tsai of CTBC University of Technology for his valuable suggestions and constructive feedback on the manuscript, which substantially improved its clarity and academic quality.

#### References

- 1 Z. Barsoum and I. Barsoum: Eng. Fail. Anal. 16 (2009) 449. https://doi.org/10.1016/j.engfailanal.2008.06.017
- 2 H.-J. Gao, Y.-D. Zhang, Q. Wu, and J. Song: Met. 7 (2017) 158. https://doi.org/10.3390/met7050158

- 3 C.-W. Kuo, C.-M. Lin, G.-H. Lai, Y.-C. Chen, Y.-T. Chang, and W. Wu: Mater. Trans. 48 (2007) 2319. <a href="https://doi.org/10.2320/matertrans.MB200706">https://doi.org/10.2320/matertrans.MB200706</a>
- 4 C.-W. Kuo, S.-M. Yang, J.-H. Chen, G.-H. Lai, and W. Wu: Sci. Technol. Weld. Joining 13 (2008) 357. <a href="https://doi.org/10.1179/174329308X299959">https://doi.org/10.1179/174329308X299959</a>
- 5 G. S. Schajer: Exp. Mech. **50** (2010) 1117. <a href="https://doi.org/10.1007/s11340-010-9386-7">https://doi.org/10.1007/s11340-010-9386-7</a>
- 6 H. Yeom, B. Choi, T. Seol, M. Lee, and Y. Jeon: Met. 7 (2017) 103. https://doi.org/10.3390/met7030103
- 7 Q. Wu, D.-P. Li, and Y.-D. Zhang: Met. 6 (2016) 80. https://doi.org/10.3390/met6040080
- K. S. Chin, S. Idapalapati, and D. T. Ardi: J. Mater. Sci. Techno. 59 (2020) 100. <a href="https://doi.org/10.1016/j.jmst.2020.03.059">https://doi.org/10.1016/j.jmst.2020.03.059</a>
- 9 S.-C. Cheng and R.-S. Lee: Sens. Mater. **37** (2025) 1891. <a href="https://doi.org/10.18494/SAM5540">https://doi.org/10.18494/SAM5540</a>
- 10 G. Xu and F. Liu: J. Mater. Sci. Eng. 13 (2025) 408. <a href="ttps://doi.org/10.3390/jmse13030408">ttps://doi.org/10.3390/jmse13030408</a>
- W. He, B. P. Gu, J. Y. Zheng, and R. J. Shen: Appl. Mech. Mater. 157–158 (2012) 1157. <a href="https://doi.org/10.4028/www.scientific.net/AMM.157-158.1157">https://doi.org/10.4028/www.scientific.net/AMM.157-158.1157</a>
- 12 C. Zeng, W. Tian, and W. H. Liao: Eng. Fail. Anal. 66 (2016) 72. https://doi.org/10.1016/j.engfailanal.2016.04.012
- Z. Barsony, A. Rutscher, and A. Kiri: 2022 IOP Conf. Ser.: Materials Science and Engineering (OATK, 2021) 12024. https://doi.org/10.1088/1757-899X/1246/1/012024
- 14 A. G. Moraes, T. G. R. Clarke, and I. L. Diehl: Mater. Res. 23 (2020). <a href="https://doi.org/10.1590/1980-5373-MR-2020-0157">https://doi.org/10.1590/1980-5373-MR-2020-0157</a>
- 15 P. Fu and C. Jiang: Mater. Des. **56** (2014) 1034. <a href="https://doi.org/10.1016/j.matdes.2013.12.011">https://doi.org/10.1016/j.matdes.2013.12.011</a>
- 16 J.-S. Wang, C.-C. Hsien, C.-M. Lin, C.-W. Kuo, and W. Wu: Metall. Mater. Trans. A 44 (2013) 806. <a href="https://doi.org/10.1007/s11661-012-1450-8">https://doi.org/10.1007/s11661-012-1450-8</a>
- 17 D. Balzar: J. Res. Natl. Inst. Stand. Technol. **98** (1993) 321. <a href="http://doi.org/10.6028/jres.098.026">http://doi.org/10.6028/jres.098.026</a>
- 18 T. Ida, S. Shimazaki, H. Hibino, and H. Toraya: J. Appl. Cryst. **36** (2003) 1107. <a href="http://doi.org/10.1107/50021889803011580">http://doi.org/10.1107/50021889803011580</a>

#### **About the Authors**



Shih-Chuan Cheng received his B.E. degree in electrical engineering from the University of Queensland, Australia, in 1999 and his M.E. degree in mold and die engineering from National Kaohsiung University of Applied Sciences, Taiwan, in 2013. He is a Ph.D. candidate at the Mechanical Engineering Department of National Cheng Kung University, Taiwan. His research interests include metal forming systems, computer-aided manufacturing, and sensor applications. (n18061054@gs.ncku.edu.tw)



Rong-Shean Lee received his Ph.D. degree in mechanical engineering from the University of Leeds, U.K. From 1982 to 2019, he was a professor at National Cheng Kung University (NCKU). Since 2019, he has been Professor Emeritus at NCKU, Taiwan. His research interests include metal forming systems, computer-aided manufacturing, applied plasticity, and intelligent manufacturing. (mersl@mail.ncku.edu.tw)